Imaging

J. Synchrotron Rad. (1998). **5**, 1079–1081

High-resolution X-ray topographic images of dislocations in a silicon crystal recorded using an X-ray zooming tube

Shigeru Kimura,[a]* Tatsuya Matsumura,[b] Katsuyuki Kinoshita,[b] Keiichi Hirano[c] and Hiroshi Kihara[d]

[a]Silicon Systems Research Laboratories, NEC Corporation, 34 Miyukigaoka, Tsukuba, Ibaraki 305, Japan, [b]Electron Tube Center, Hamamatsu Photonics KK, 314-5 Shimokanzo, Toyooka, Iwata-gun, Shizuoka 438-01, Japan, [c]Photon Factory, High Energy Accelerator Research Organization, 1-1 Oho, Tsukuba, Ibaraki 305, Japan, and [d]Kansai Medical University, 18-89 Uyama-Higashi, Hirakata, Osaka 573, Japan. E-mail: kimuras@lbr.cl.nec.co.jp

(*Received 4 August 1997; accepted 30 October 1997*)

A Be-window-type X-ray zooming tube is an X-ray digital imaging system whose magnification factor of X-ray images can be easily varied from 10 to 200, and whose spatial resolution is less than 0.5 μm. This zooming tube was used as an imaging detector in double-crystal X-ray topography to obtain high-resolution images of dislocations in a silicon crystal. X-ray interference images of about 5 μm were observed even though optimal performance of the X-ray zooming tube could not be achieved. The results indicate that the X-ray zooming tube might make a good detector for X-ray topography with minor improvements in its stage structure.

Keywords: X-ray topography; X-ray zooming tubes; X-ray imaging systems; digital images; silicon; dislocations.

1. Introduction

The X-ray zooming tube is an imaging system developed for the measurement of X-ray images at the microscopic level (Kinoshita, Matsumura, Inagaki, Hirai, Sugiyama, Kihara, Watanabe & Shimanuki, 1992; Kinoshita, Matsumura, Inagaki, Hirai, Sugiyama, Kihara, Watanabe, Shimanuki & Yagishita, 1992). This system has several advantages such as (i) high-spatial resolution of less than 0.5 μm, (ii) easy variation of the magnification factor from 10 to 200, (iii) straightforward searching of the field of view, (iv) high sensitivity over a wide X-ray energy range from 80 to 20 keV, (v) real-time and accumulated imaging, and (vi) data acquisition in a digitized form for each constituent pixel. Because of these characteristics, the X-ray zooming tube has been used as an imaging tool for soft X-ray contact microscopy (Watanabe *et al.*, 1993; Ito *et al.*, 1996), soft X-ray imaging microscopy (Ohsuka *et al.*, 1992) and soft X-ray holographic microscopy (Shinohara *et al.*, 1996). However, few applications have been reported in hard X-ray imaging even though the X-ray zooming tube has sufficient sensitivity in the hard X-ray region. This is because the X-ray zooming tube was designed for in-vacuum experiments, so samples had to be set in a vacuum chamber that was directly connected with the X-ray zooming tube by a flange. This made hard X-ray experiments, which are usually performed in air, difficult.

Recently, Matsumura *et al.* (1997) developed a Be-window-type X-ray zooming tube that enables samples to be set in air, and demonstrated that an absorption image of more than 0.3 μm-wide zones of a zone plate could be observed at an X-ray energy of 20 keV. This indicates that the Be-window-type X-ray zooming tube can also be used as a detector in X-ray topography. In the present work, therefore, we used the Be-window-type X-ray zooming tube as a detector in double-crystal X-ray topography using 11.024 keV X-rays, and sought to obtain high-resolution images of dislocations in a silicon crystal. X-ray interference images of about 5 μm were observed. However, optimal performance of the X-ray zooming tube could not be achieved because the distance from the sample to the Be window of the X-ray zooming tube was limited to over 400 mm due to the stage structure of the zooming tube. Since the X-ray zooming tube has some advantages compared with nuclear emulsion plates, *e.g.* development and fixation processes are not required and digitizing of the observed images is easy, it might make a good detector for X-ray topography with minor improvements in its stage structure.

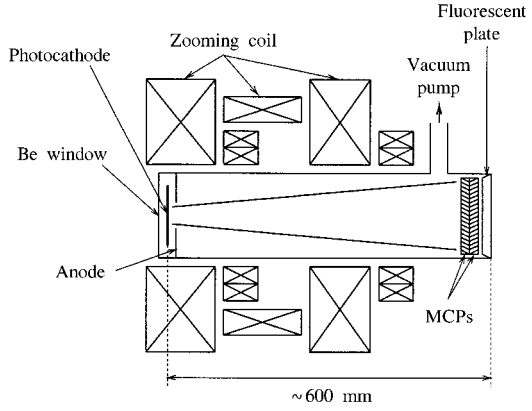

Figure 1
Schematic diagram of the Be-window type X-ray zooming tube.

2. Experimental procedure

2.1. *The Be-window-type X-ray zooming tube*

The Be-window-type X-ray zooming tube we used is shown schematically in Fig. 1. It consists of a photocathode, an electron lens, an electron multiplier, and a fluorescent screen. The X-rays that pass through the 0.1 mm-thick Be window are converted to photoelectrons by the CsI photocathode, which has an effective diameter of 2.5 mm and a thickness of 300 nm. The CsI was evaporated on a 30 nm-thick gold substrate formed on a 100 nm-thick organic film. The quantum efficiency (emitted photoelectrons/input photons) of the CsI photocathode has been measured within an energy range from 80 to 10 keV by Kinoshita, Matsumura, Inagaki, Hirai, Sugiyama, Kihara, Watanabe & Shimanuki (1992). In the present case (X-ray energy of 11.024 keV), the quantum efficiency is expected to be about 1.0, which is almost the same as that at 10 keV. The photoelectrons are magnified by the electron lens, multiplied by the two micro-channel plates (MCPs), then converted to visible light on the fluorescent screen. These visible-light images were recorded with a conventional CCD camera. The magnification ratio of the images on the

fluorescent screen can be changed continuously between 10 and 200 without adjusting the sample or the X-ray optics system. In addition, any desired position on the photocathode can be magnified for observation by using a deflection function.

2.2. *Double-crystal X-ray topography*

The experimental arrangement was set up at BL-15C of the Photon Factory at the High Energy Accelerator Research Organization (KEK), Tsukuba, Japan (Fig. 2) (Ishikawa, 1989; Kimura & Ishikawa, 1995). X-rays with an energy of 11.024 keV were selected with a double-crystal monochromator using flat Si(111) crystals. The X-rays are collimated by an Si(111) crystal using 008 asymmetric reflection. Since the angle, α, between the collimator crystal surface and the diffraction plane is 55.90°, the asymmetric factor b [= sin ($\theta_B - \alpha$) / sin ($\theta_B + \alpha$)], was calculated to be about 0.02. Thus, the angular divergence of the X-ray beam from the collimator crystal is reduced to about 0.13″. A sample was prepared from a ⟨001⟩-oriented Czochralski-grown Si crystal with dislocations. A half-circle-shaped wafer with a diameter of about 25 mm and a thickness of about 5 mm was used. The sample was aligned to provide 008 symmetric reflection, thereby allowing an (n, $-n$) nondispersive setting. To determine the exact peak angle, an 008 diffraction profile was measured with a 0.02″ step size for the central part of the sample, as determined by the 1 mm-diameter aperture. To take topographs, the X-rays reflected from the sample at two offset angles were converted to video images by using the Be-window-type X-ray zooming tube combined with a conventional CCD camera. The detected images were processed by an image processor, and monitored using a TV monitor screen. For comparison, topographs were also recorded on Ilford L4 nuclear emulsion plates, which are usually used as an imaging detector for high-resolution X-ray topography.

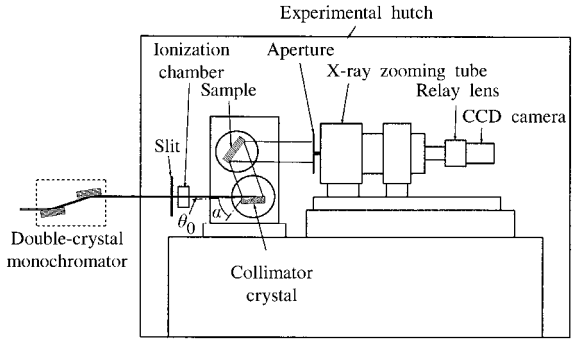

Figure 2
Schematic diagram of the experimental arrangement set-up at beamline 15C of the Photon Factory. Here, θ_0 and α represent the glancing angle to the sample surface and the angle between the sample surface and the diffraction plane, respectively.

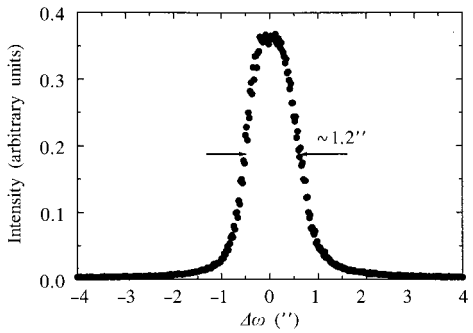

Figure 3
A measured 008 diffraction profile.

3. Results and discussion

The measured 008 diffraction profile of the sample is shown in Fig. 3, where $\Delta\omega$ represents the offset angle from the peak angular position. The full width at half-maximum (FWHM) of the curve is about 1.2″. Topographic images of a dislocation in the sample recorded on the nuclear emulsion plates and the X-ray zooming tube are shown in Figs. 4 and 5, respectively. Both sets of images were taken at $\Delta\omega$ of (a) +1.0″ and (b) +4.0″. In Fig. 4, the dislocation image becomes narrower as $\Delta\omega$ increases. This is because the sensitivity to the strain field around defects becomes lower as $\Delta\omega$ becomes larger. Therefore, an interference fringe image of about 5 μm reflected from the weak strained region is observed in Fig. 4(a) and a direct image with a minimum width of about 2 μm reflected from the strongly strained region is observed in Fig. 4(b). On the other hand, even though the interference fringe image of about 5 μm can be observed in Fig. 5(a), the recorded images are blurred to more than 10 μm in Fig. 5(b). This is because the distance from the sample to the Be window of the X-ray zooming tube was limited to over 400 mm

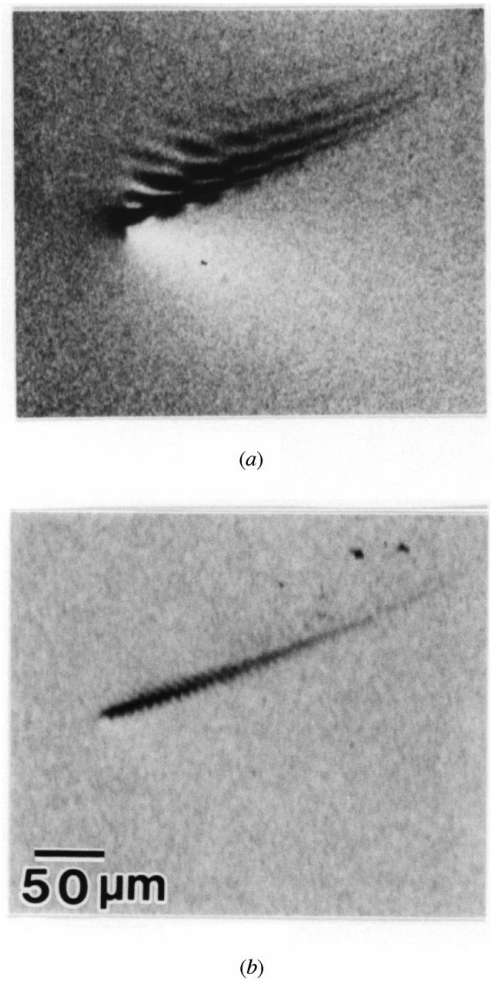

(a)

(b)

Figure 4
A series of topographic images of the dislocation recorded using the nuclear emulsion plates. These were taken at $\Delta\omega$ of (a) +1.0″ and (b) +4.0″.

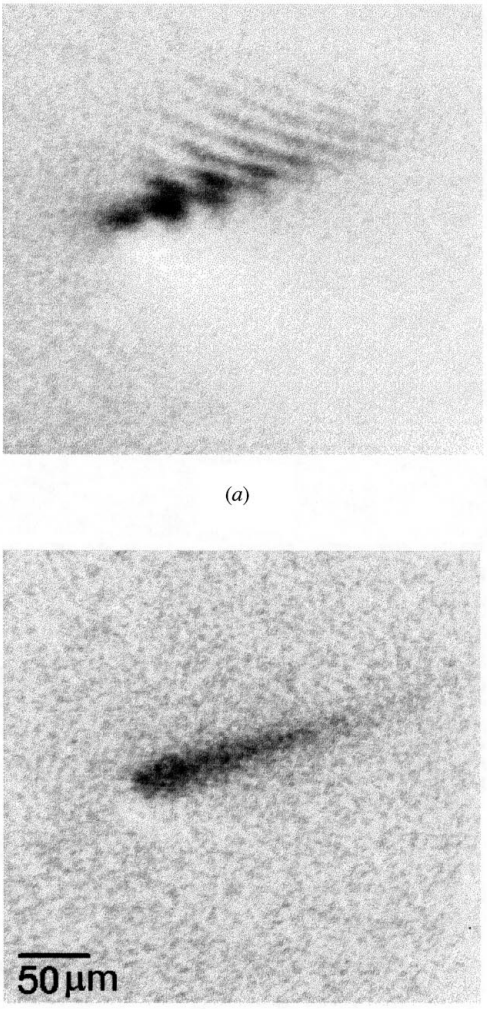

Figure 5
A series of topographic images of the dislocation recorded using the Be-window-type X-ray zooming tube. These were taken at $\Delta\omega$ of (*a*) +1.0″ and (*b*) +4.0″.

due to the stage structure of the zooming tube; the nuclear emulsion plates, on the other hand, were placed 50 mm from the sample position. Since the reflected X-ray divergence from the strongly strained region is larger than that from the weakly strained region, the direct image is very blurred while the interference fringe image is clearer. Differences in the distance from the sample position also affected the exposure times. Exposure times for Fig. 4 were (*a*) 2 min, (*b*) 6 min, and those for Fig. 5 were (*a*) 100 min, (*b*) 600 min, indicating that the exposure time needed with the X-ray zooming tube is more than one hundred times as long as with the plates. However, considering that the photon density of the reflected X-rays falls off at the inverse square of the distance, we believe that the actual detection sensitivity of the X-ray zooming tube is about one-half that of the nuclear emulsion plate.

4. Concluding remarks

We used the Be-window-type X-ray zooming tube as a detector in double-crystal X-ray topography using 11.024 eV X-rays to obtain high-resolution images of dislocations in a silicon crystal. X-ray interference images of about 5 μm were observed. However, optimal performance of the X-ray zooming tube could not be achieved because the distance from the sample to the Be window of the X-ray zooming tube was limited to over 400 mm due to the stage structure of the zooming tube. To obtain higher resolution images of less than 1 μm, we simply have to shorten the distance from the sample to the X-ray zooming tube. Since the X-ray zooming tube offers advantages compared with nuclear emulsion plates, *e.g.* development and fixation processes are not required and digitizing of the observed images is easy, it should prove to be a good detector for X-ray topography with minor improvements in its stage structure.

This work was performed using synchrotron radiation at the Photon Factory, High Energy Accelerator Research Organization, under the approval of the Photon Factory Advisory Committee (proposal Nos. 95-P012 and 95-C002).

References

Ishikawa, T. (1989). *Rev. Sci. Instrum.* **60**, 2490–2493.
Ito, A., Shinohara, K., Nakano, H., Matsumura, T. & Kinoshita, K. (1996). *J. Microsc.* **181**, 54–60.
Kimura, S. & Ishikawa, T. (1995). *J. Appl. Phys.* **77**, 528–532.
Kinoshita, K., Matsumura, T., Inagaki, Y., Hirai, N., Sugiyama, M., Kihara, H., Watanabe, N. & Shimanuki, Y. (1992). *Proc. SPIE*, **1741**, 287–293.
Kinoshita, K., Matsumura, T., Inagaki, Y., Hirai, N., Sugiyama, M., Kihara, H., Watanabe, N., Shimanuki, Y. & Yagishita, A. (1992). *X-ray Microscopy III*, edited by A. Michette, G. Morrison & C. Buckley, pp. 335–337. Berlin: Springer-Verlag.
Matsumura, T., Kinoshita, K., Tamura, S., Kamijo, N., Ozaki, Y. & Kihara, H. (1997). *X-ray Microscopy and Spectromicroscopy*, edited by J. Theme, G. Schmahl, E. Umbach & D. Rudolph. Berlin: Springer-Verlag. In the press.
Ohsuka, S., Ohba, A., Sugiyama, M., Hayakawa, T., Matsumura, T., Kinoshita, K., Watanabe, N., Shimanuki, Y., Sano, Y. & Kihara, H. (1992). *X-ray Microscopy III*, edited by A. Michette, G. Morrison & C. Buckley, pp. 335–337. Berlin: Springer-Verlag.
Shinohara, K., Ito, A., Nakano, H., Kodama, I., Honda, T., Matsumura, T. & Kinoshita, K. (1996). *J. Synchrotron Rad.* **3**, 35–40.
Watanabe, N., Matsumura, T., Inagaki, Y., Kinoshita, K., Shimanuki, Y., Furuya, K., Taguchi, T., Taniguchi, M. & Kihara, H. (1993). *J. Microsc.* **170**, 141–146.